

Postglacial palaeoenvironmental reconstruction of the Fury and Hecla Strait region (Nunavut) inferred from microfossils and geochemical proxies

MARC-ÉLIE ADAÏMÉ,^{1*} REINHARD PIENITZ,¹ PIERRE LEGENDRE² and DERMOT ANTONIADES¹

¹Laboratoire de Paléocéologie Aquatique, Centre d'études Nordiques & Département de Géographie, Takuvik Joint International Laboratory, Université Laval (Canada)–CNRS (France), Université Laval, Québec, Québec, Canada

²Département de sciences biologiques, Université de Montréal, Montréal, Québec, Canada

Received 3 July 2020; Revised 19 January 2021; Accepted 6 February 2021

ABSTRACT: An analysis of sediment records from two lakes located along the southeastern shore of the Fury and Hecla Strait (Nunavut, Canada) allowed us to reconstruct the regional environmental history since deglaciation. Multiproxy profiles, namely particle-size distribution, elemental geochemistry (based on X-ray fluorescence) and diatom assemblages, revealed a regional deglaciation and marine inundation around 8200 cal a BP. This suggests that glacial retreat in this region likely occurred several hundred years earlier than previously extrapolated. At that time, the connection between the Atlantic and Pacific Ocean currents must have been established and glacial isostatic adjustment gradually isolated the lacustrine basins from marine influence. Diatom assemblages revealed an abrupt marine–brackish–freshwater transition (ca. 6670–6130 cal a BP) through a shift in dominance from initial polyhalobian (e.g. *Tabularia fasciculata*, *Navicula directa*), intermediate mesohalobian (e.g. *Cyclostephanos dubius*, *Thalassiosira baltica*) to oligohalobian (fragilarioid *Staurosirella pinnata*, *Staurosira venter*, *Pseudostaurosira pseudoconstruens*, *P. brevistriata*) taxa. Multivariate analyses (redundancy analysis and multivariate regression tree) conducted on the biological and litho-geochemical data also suggest that climatic conditions may have remained relatively warm throughout the interval ~6000–3900 cal a BP, before significantly cooling over the past few millennia, as inferred from a decrease in organic matter accumulation and shifts in diatom communities. Copyright © 2021 John Wiley & Sons, Ltd.

KEYWORDS: deglaciation; diatoms; elemental geochemistry; micropalaeontology; palaeogeography; palaeolimnology

Introduction

The scarcity of studies conducted in polar regions makes palaeolimnology a valuable discipline that allows the development and use of new physical, chemical, biological and numerical tools, testing climate models and unravelling important details of past environments. This is especially true in the context of accelerated global change driving abrupt environmental and ecological shifts at high latitudes.

The Fury and Hecla Strait, for instance, has drawn little scientific attention so far, despite its key importance stemming from its strategic geographic location at the confluence of the Atlantic Ocean currents coming from the Foxe Basin to the south and those arriving from the Pacific Ocean through the Gulf of Boothia in the north (Fig. 1). The region's Holocene environmental history has been shaped by extensive Wisconsinan glacial activity, followed by the gradual withdrawal of the Laurentide Ice Sheet and the onset of important palaeogeographical and geophysical changes, including marine inundation and the beginning of glacial isostatic adjustment. These dynamics are well documented, as several studies (Sim, 1960; Ives and Andrews, 1963; Dyke and Prest, 1987) have reconstructed ice flows originating from the Foxe Ice Dome, following a dominant westward direction, in addition to a late southwestward flow from Baffin Island at 8500 ¹⁴C a BP (Dredge, 2001; Dyke, 2008). Deglaciation subsequently led to the formation of several lakes occupying

rock basins scooped out by glacial erosion (Dredge, 2001). Prior studies (e.g. Dredge, 1990, 2001; Dyke, 2004, 2008) have suggested a glacial chronology for the Fury and Hecla Strait region based exclusively on extrapolation of radiocarbon dates of raised beaches rather than *in situ* records. Dyke et al. (1996) and Dyke (2004) placed this interval between 7000 and 6000 ¹⁴C a BP (7800 and 6850 cal a BP), whereas Dredge (2001) proposed that areas more distant from the Foxe Ice Dome centre, including the strait itself, were deglaciated after 6900 ¹⁴C a BP (7750 cal a BP). Dyke (2008), however, indicated that the Fury and Hecla flow was operating by 8500 ¹⁴C a BP (9500 cal a BP) and remained active until after 6500 ¹⁴C a BP (7400 cal a BP). While such results do not yield precise conclusions regarding the postglacial evolution of the region, they nevertheless provide valuable palaeogeographical context.

The main objectives of this study were to understand the palaeogeographical history of the region since deglaciation, including the timing of glacial retreat and lake formation, and to examine the relationship between environmental fluctuations and biological shifts throughout the Holocene.

To address these questions, we applied a multiproxy approach based on changes in particle-size distribution, elemental geochemistry and diatom microfossil assemblages in sediment cores. The relevance of this study stems from the aforementioned scarcity of palaeolimnological data in the region as well as the strategic location of the Fury and Hecla Strait as a 'gateway' between Atlantic and Pacific waters, making it an ideal place to yield insights into questions in various fields, such as palaeoceanography, biogeography, palaeoanthropology and palaeogenetics.

*Correspondence: M.-É. Adaimé, as above.
E-mail: madaime2@illinois.edu



Figure 1. Location of the Fury and Hecla Strait at the confluence of the Atlantic (red arrow) and Pacific (blue arrow) ocean currents via Foxe Basin and the Gulf of Boothia. [Color figure can be viewed at [wileyonlinelibrary.com](https://onlinelibrary.wiley.com)]

A precise postglacial chronology of events, such as regional deglaciation and the opening of the strait, would serve as a valuable reference point for studies dealing with Palaeo-Eskimo migrations and faunal and floral exchanges between two major ocean water masses (intermixing of ocean biota), among many other questions (McGhee, 1976; Dyke et al., 2011; Coad and Reist, 2018).

Regional setting

Local geology and geomorphology

The Fury and Hecla Strait geological group consists of siliciclastic and volcanic rocks overlying Archean and Palaeoproterozoic crystalline bedrock (Patzke et al., 2018). This formation is composed mainly of granitoid gneiss, mafic intrusions and minor metasedimentary rocks, also described by Dredge (2001) as Proterozoic sandstone/quartzite rocks near the northernmost end of the Melville Peninsula. Late Wisconsinan glacial dynamics have triggered profound changes in various regional geomorphological features recorded by the presence of glacially polished and striated rocks, extensive till plains occupying a large proportion of the region and several shallow lakes of glacial origin (Dredge, 2001). Among these, our two study lakes were located in a zone of continuous permafrost. Both lakes were ultra-oligotrophic, as is typical of Arctic waterbodies (Table 1). Lake Fury 1 (unofficial name; 69°41'11" N, 83°09'24" W) is located 204 m above sea level (asl) and 1.15 km south of the Fury and Hecla Strait, whereas Lake Fury 2 (unofficial name; 69°39'42" N, 82°33'12" W) is located 65 m asl, 2.70 km south of the strait (Fig. 2). The lakes have maximum depths of 32.5 and 20.9 m, respectively.

Catchment vegetation

Terrestrial vegetation in the lake watersheds was scarce. Although vegetation was slightly denser around Lake Fury 1, specific diversity was low. While surveys have indicated the presence of a prostrate/hemiprostrate dwarf-shrub tundra in the region, marked by species such as *Cassiope tetragona*, *Rhododendron lapponicum* and *Salix arctica* (Walker et al., 2005), our observations noted the dominance of only a few low-growing shrubs, such as *Salix arctica* and *Salix polaris*, sparsely populating an exposed lichen-covered bedrock.

Table 1. Results of limnological measurements and water chemistry analyses from lakes Fury 1 and Fury 2, sampled on 31 August and 1 September 2017, respectively

Variable	Fury 1	Fury 2
pH	7.56	7.70
Calcium (mg/L)	6.34	8.62
Chloride (mg/L)	2.5	4.7
Silica (mg/L)	0.36	0.19
Total phosphorus (µg/L)	2.5	4.0
Total dissolved phosphorus (µg/L)	0.8	1.6
Dissolved inorganic carbon (mg/L)	6.0	8.1
Dissolved organic carbon (mg/L)	0.9	1.6
Specific conductivity (µS/cm)	58.2	88.4
Surface temperature (°C)	6.71	6.87
Temperature near bottom (°C)	6.72	6.86
Secchi disc depth (m)	12	11
Maximum depth (m)	32.5	20.9
Threshold elevation (m asl)	204	65
Surface area (km ²)	0.09	0.11



Figure 2. Lakes Fury 1 (left) and Fury 2 (right), located 1.15 and 2.70 km from the Fury and Hecla Strait, respectively (photo credit: Reinhard Pienitz). [Color figure can be viewed at wileyonlinelibrary.com]

Regional climate

The climate in Igloodik (Nunavut), 40–50 km from our study site, is characterised by an average annual temperature of -12.9°C (July = 7.6°C) and mean annual precipitation of 275 mm (Environment Canada, 2019).

Methods

Field sampling

Sediment cores were collected during summer 2017 (31 August and 1 September), based on the hypothesis that postglacial changes would be recorded in lake sediments through biological, physical and geochemical proxies. Bathymetric surveys were conducted in both lakes using a portable sonar (Humminbird 859 CI HD) equipped with an internal GPS, and cores were taken from the lakes' deepest parts, using a 7 cm diameter percussion corer (Aquatic Research Instruments). Core Fury-1 (70 cm) was extracted from Lake Fury 1 and comprised marine and freshwater sediments. It was mainly used to confirm the regional postglacial chronology. Fury-2F (59 cm) was extracted from Lake Fury 2 and consisted only of lacustrine sediments. It was complementary to the longer core Fury-2C (82 cm) extracted from the same lake. The latter served as the main study archive to reconstruct postglacial palaeoenvironmental conditions in the region.

Geochronology

Seven accelerator mass spectrometry (AMS) ^{14}C dates were obtained from cores Fury-1 (one date) and Fury-2C (six dates) (Table 2), all of which were measured on bulk organic sediments, with the exception of two samples of bryophyte remains extracted from the basal, inorganic glacio-marine sections of cores Fury-1 and Fury-2C. Samples were prepared at the Centre for Northern Studies Radiochronology Laboratory and measured at the Keck Carbon Cycle AMS Facility.

An age–depth model for Fury-2C based on Bayesian inference was generated using the rbacon package in R

(Blaauw and Christen, 2019). The core was divided into several equally spaced sections and sediment accumulation rates (a cm^{-1}) were estimated for each section through millions of Markov Chain Monte Carlo iterations (Blaauw and Christen, 2011).

Lithology

Cores were taken to the Institut national de la recherche scientifique (INRS-EET, Québec, Canada) for non-destructive measurements of density variations using a computed tomography scanner (Siemens SOMATOM Definition AS). The cores were then split lengthwise and analysed with an Itrax X-ray fluorescence (XRF) core scanner at 500 μm intervals with an exposure time of 10 s per point. Profiles of elements with low signal-to-noise ratios were removed, resulting in the inclusion of those seen in Figs. 4, 5 and 6. The values, originally expressed in peak area integrals, were then normalised to kilocounts per second (kcps) in order to account for the irregular nature of the sediment matrix (Cuven et al., 2011). The results were then averaged at 1 cm resolution for statistical comparability, and elements displaying relatively high signal-to-noise ratios (i.e. Si, K, Ca, Ti, Mn and Fe) were selected for further analyses. Elemental ratios (i.e. Ca/Ti and Mn/Ti) were calculated and used as supplementary (passive) palaeoenvironmental proxies for potential variations in biogenic carbonate and bottom-water oxygenation, respectively. Ca/Ti is used as a palaeoproductivity proxy and was shown to be correlated with other biomass indicators such as total organic carbon and, to some extent, temperature (Kylander et al., 2013). Mn/Ti, on the other hand, has been used for tracing past redox conditions (Croudace et al., 2006; Kanamaru et al., 2013; Kylander et al., 2013; Davies et al., 2015), with low values (associated with anaerobic conditions) pointing to either lower oxygenation at the water–sediment interface following lake stratification, or water deoxygenation induced by organic decay during periods of high biological productivity (Davies et al., 2015). Significant stratigraphic zones were determined according to the broken stick model and the constrained incremental sum of

Table 2. AMS ^{14}C dates of samples extracted from cores Fury-1 and Fury-2C. Most dates were obtained on bulk organic sediment (gyttja), with the exception of samples Fury 1-57 and Fury 2-76, dated on bryophyte remains found in glacio-marine sediments. ^{14}C dates used in the rbacon package are shown by a dagger

Laboratory number	Sample number	Core depth (cm)	Material	^{14}C date (a BP)	2σ age range (cal a BP)	Calibrated a BP (median probability)
ULA-8292	Fury 1-57	56.5–57	Bryophytes	7275 ± 20	8020–8160	8100
ULA-7769	Fury 2-17	17–17.5	Bulk sediment	$2980 \pm 15^\dagger$	3070–3280	3180
ULA-7770	Fury 2-31	31–31.5	Bulk sediment	$3610 \pm 15^\dagger$	3800–4060	3960
ULA-7771	Fury 2-43	43–43.5	Bulk sediment	$4700 \pm 15^\dagger$	5240–5600	5390
ULA-7766	Fury 2-56	56–56.5	Bulk sediment	$5455 \pm 20^\dagger$	6110–6930	6510
ULA-7767	Fury 2-57	57–57.5	Bulk sediment	$6025 \pm 15^\dagger$	6340–6980	6670
ULA-8175	Fury 2-76	76–77	Bryophytes	$7375 \pm 25^\dagger$	8160–8310	8190

squares algorithm, implemented in the package rioja in R (Juggins, 2019).

Magnetic susceptibility (MS), used to assess potential changes in minerogenic input (Lie et al., 2004), was also measured throughout core Fury-2C at 0.5 cm intervals using the sensor incorporated into the Itrax core scanner system and averaged at 1 cm resolution.

Organic matter and water content

Core Fury-2C was subsampled at 0.5 cm intervals and samples were placed in individual Whirl-Pak bags. All 164 samples were weighed, then freeze-dried for a minimum of 48 h, and weighed again to calculate water content throughout the core.

The samples were then analysed by loss-on-ignition to estimate organic matter content. Freeze-dried samples of approximately 0.30 g were transferred into pre-weighed crucibles and heated to 550 °C for 4 h according to the method of Heiri et al. (2001).

Grain-size analysis

The sedimentological properties of core Fury-2C were analysed with an LA-960 Horiba Laser Particle Size Analyzer to reconstruct changes in particle input to the lake. Samples were prepared by adding a solution of 10% (NaPO₃)₆ (as a dispersing agent) to the LOI₅₅₀ samples at 1 cm intervals and the solution was kept at room temperature for 24 h. Particle-size distribution, based on multiple measurements, was determined for every sample. The average size, as well as the spread (sorting) values of the sediments, were then calculated based on the arithmetic method of moments using the GRADISTAT program (Blott and Pye, 2001).

Diatom analyses

A 0.05 mg subsample of freeze-dried sediment was extracted from 66 samples at 1 cm intervals (core Fury-2C) for diatom analysis that followed standard procedures as outlined in Pienitz et al. (1995). Samples were treated with strong acids (H₂SO₄ and HNO₃ 1:1 (v/v)) to digest the organic sediment matrix. Permanent microscope slide mounts were then prepared using the synthetic resin Naphrax. Diatom species were identified along random transects on the slides using a Zeiss Axio Imager 2 microscope at a magnification of 1000–1500×. At least 300 diatom valves were counted for each depth, with the exception of eight samples with low valve densities. Damaged valves were only included in the enumeration process when distinctive parts of the species were present. Diatoms were identified to the lowest taxonomic level possible based on published floras (Krammer and Lange-Bertalot, 1991a, 1991b; Campeau et al., 1999; Fallu et al., 2000; Antoniadis et al., 2008; Zimmermann et al., 2010). Species relative abundances were calculated, and taxa were included in a percentage diagram and organised according to their salinity preferences as indicated by Campeau et al. (1999).

Alpha diversity, used to assess diversity of species composition at individual sites (Legendre and Legendre, 2012), was estimated using the exponential of Shannon entropy H (uncertainty associated with a frequency distribution p), given by:

$$D = \exp\left(-\sum_{i=1}^S p_i \ln p_i\right) = \exp(H) \quad (1)$$

Evenness was also calculated to assess the degree of homogeneity in the distribution of species using the index proposed by Smith and Wilson (1996). Based on the variance in abundances over the species, it was computed as follows:

$$E_{var} = 1 - \frac{2}{\pi} \arctan \left\{ \frac{\left(\sum_{i=1}^S \left[\ln(p_i) - \sum_{j=1}^S \ln(p_j) / S \right]^2 \right)}{S} \right\} \quad (2)$$

where S is the taxa richness and p_i the relative abundance of taxon i . E_{var} varies from 0, when the sample is dominated by a single taxon, to 1, when all taxa are equally abundant.

Numerical analyses

Multivariate analyses were conducted on the lacustrine section of core Fury-2C to explore environmental change over time. A principal component analysis (PCA) was performed on all measured palaeoenvironmental variables (standardised at the beginning of the calculation) using the function PCA of the package FactoMineR in R (Husson et al., 2019). This increased the dataset interpretability and helped us examine possible correlations among explanatory variables (potentially driving changes in diatom communities) comprising the geochemical and lithological data. Elemental ratios (Ca/Ti and Mn/Ti) were included in the analysis as supplementary proxies. Variables were plotted on the PCA ordination (axes 1 and 2) within a circle of radius 1, and the cumulative R² (goodness-of-fit statistics) of each variable's representation on the first two components was computed using the goodness function of the package vegan (Table 3) (Oksanen et al., 2019). A PCA was also used in combination with hierarchical clustering to assign PCA scores to all observations and group them into meaningful clusters using the HCPC function of FactoMineR.

A redundancy analysis (RDA) (the canonical form of PCA) was conducted to explore potential species–environment relationships along the lacustrine section of core Fury-2C. The explanatory matrix included both the lithological and geochemical variables integrated in the PCA, as well as two linearly interpolated Holocene mean July temperature records inferred from pollen assemblages collected near our study site (Gajewski, 2015). The response matrix consisted of diatom relative abundance data, which were Hellinger-transformed prior to the analysis to render them suitable for linear ordination methods based on Euclidean distances (Legendre and Gallagher, 2001). The 13 environmental variables were forward-selected through 9999 permutations, and Bonferroni corrections were applied to

Table 3. Cumulative R² of the variables' representations on the first two principal components (i.e. axes 1 and 2) in the principal component analysis of zone 3 (lacustrine section) in core Fury-2C

Variable	Cumulative R ²
Fe	0.83
Mn	0.94
Ti	0.98
K	0.98
Ca	0.83
Si	0.84
Mean size	0.59
Sorting	0.70
LOI ₅₅₀	0.90
Water content	0.80
Magnetic susceptibility	0.47

probability values for a more rigorous selection. Only statistically significant variables ($P < 0.01$) were included in the RDA, generated using the `rda` function of `vegan`. The overall significance of the canonical relationship (R^2) was tested with the `anova.cca` function of the same package. The RDA triplot was produced using a scaling type 2 to emphasise the covariances among the species (Legendre and Legendre, 2012).

A multivariate regression tree (MRT) was also generated using the package `mypart` in R, to model and predict species–environment relationships based on the sums of squared deviations from the group means of the response data as proposed by De'ath (2002). The MRT represents a powerful, complementary tool to canonical analyses such as the RDA and forms clusters based on repeated splitting of the data (De'ath, 2002; Larsen and Speckman, 2004; Legendre and Legendre, 2012). The model selects explanatory variables that most strongly influence the response matrix (biological communities) and each of these variables x_{ij} controls a binary split N of the response data (defined by a threshold t) of the form:

$$N_1 = \{i \in N : x_{ij} < t\}, N_2 = \{i \in N : x_{ij} \geq t\} \quad (3)$$

The earlier the variable controls the split, the more prominent and predictive it is. The final result is a series of binary decisions leading to different leaves, each characterised by a bar plot reflecting species assemblages, its number of samples and relative error (Borcard et al., 2011). The optimal tree size was selected according to the lowest cross-validation relative error (CVRE), corresponding to the ratio of the dispersion unexplained by the tree to the total dispersion of Y , hence indicating the model's predictive power, and computed as follows:

$$CVRE = \frac{\sum_{i=1}^n \sum_{j=1}^p (y_{ij(k)} - \hat{y}_{j(k)})^2}{\sum_{i=1}^n \sum_{j=1}^p (y_{ij} - \bar{y}_j)^2} \quad (4)$$

where $y_{ij(k)}$ is one observation of the test set k , $\hat{y}_{j(k)}$ is the predicted value of one observation in one leaf (centroid of the observations of that leaf), and the denominator represents the overall dispersion (sum of squares) of the response data (De'ath, 2002; Borcard et al., 2011).

Results

Chronology

The Bayesian age–depth model, spanning a time interval of 8700 cal a BP (Fig. 3), was generated with the six ^{14}C samples from core Fury-2C. The model showed a relatively stable accumulation rate at the base of the core, but this rate decreased from 94 a cm^{-1} , between 82 and 30 cm, to 131 a cm^{-1} from 30 cm upwards.

Stratigraphy

• Core Fury 1

Core Fury 1 was characterised by a bottom section (at least 8100 cal a BP) consisting of yellow-brown sandy silt, rich in macrofloral remains. The section was overlain by a thick organic-rich unit, also marked by a sharp transition from 33 cm upwards towards slightly less organic conditions (Fig. 4).

• Core Fury-2F

Core Fury-2F consisted only of organic-rich sediments. However, a change in its composition (characterised by a thin sandy silt layer) punctuated its 31 cm horizon, followed by an upward transition towards slightly lighter-coloured sediments (Fig. 5).

• Core Fury-2C

Like core Fury 1, Fury-2C contained very fine, light-coloured sandy silt at its base (at least 8200 cal a BP). This section was overlain by a transitional unit beginning with a dark brown layer, followed by an upper section of laminated organic-rich sediments 4 cm thick. The latter section also reflected lithological changes at 30 cm, marking a clear transition towards lighter-coloured sediments upcore (Fig. 6).

Elemental geochemistry

• Core Fury-1

There were three statistically significant geochemical zones in core Fury-1 (Fig. 4): (1) a bottom mineral section (70–55 cm); (2) a thick intermediate organic-rich section (55–33 cm); followed by (3) an upper section of markedly less organic sediments (33–0 cm).

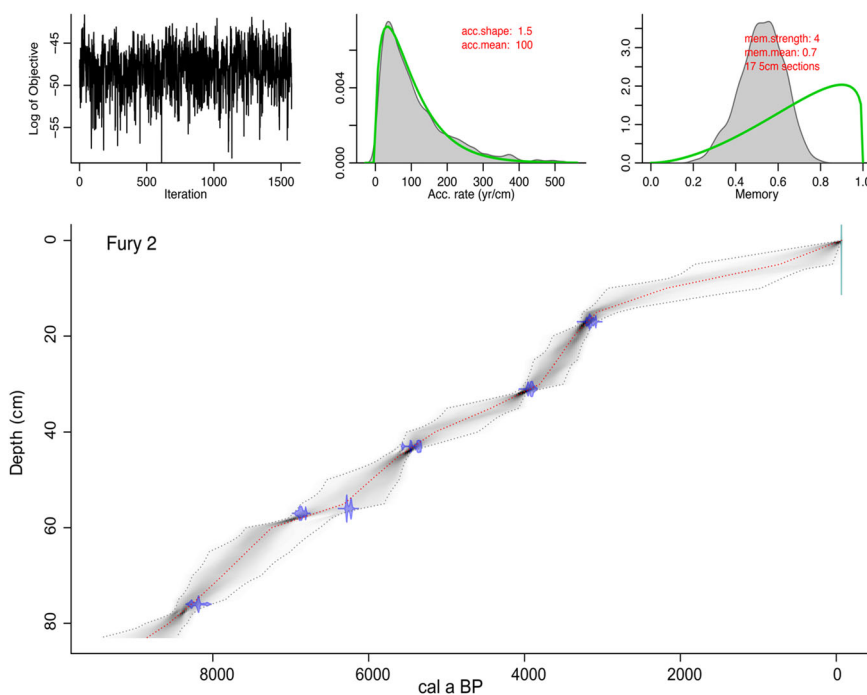


Figure 3. Bayesian age–depth model of core Fury-2C, generated using the `Bacon` function in R. The blue symbols represent the six AMS ^{14}C dates, bounded by the grey dots showing the model's 95% confidence intervals. The red central line represents a second-order polynomial regression fit, indicating the best model (the most likely date) based on the weighted mean average. [Color figure can be viewed at wileyonlinelibrary.com]

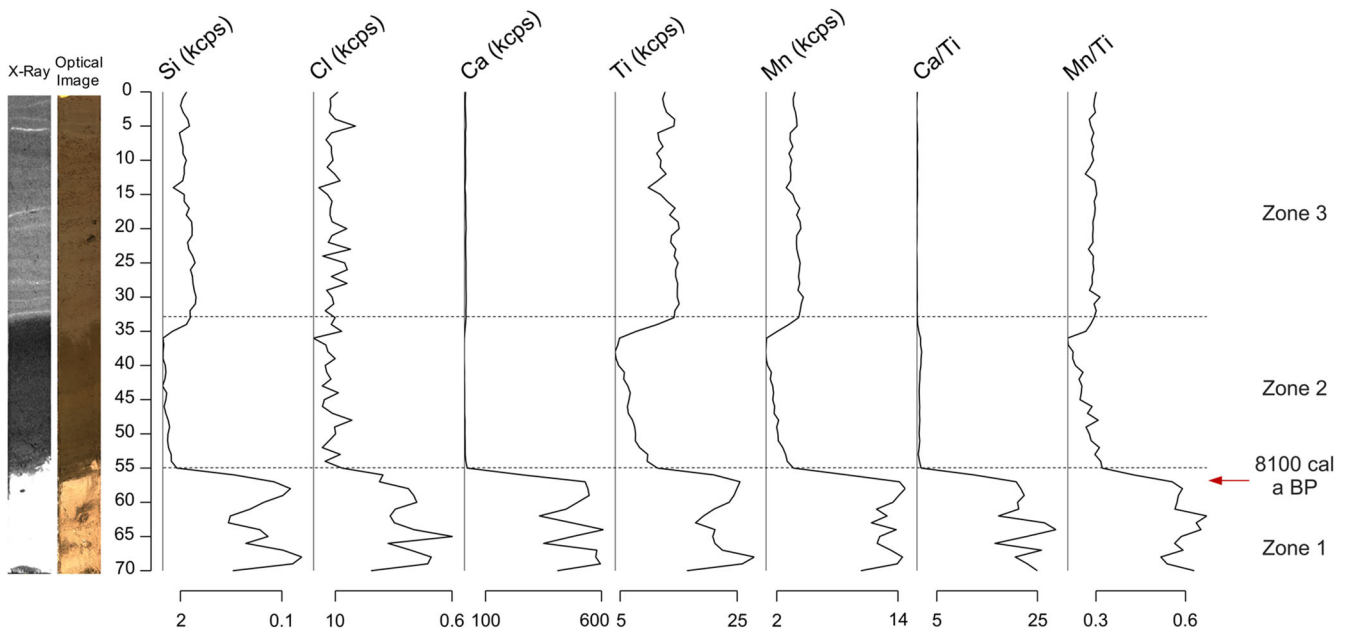


Figure 4. Averaged (i.e. 1 cm averages) geochemical profiles throughout core Fury-1, including elemental ratios reflecting biomass (Ca/Ti) and redox (Mn/Ti) conditions. Elements such as K and Fe were not plotted given their high correlation with Ti and Mn. The lighter and darker shades of grey on the X-ray image reflect higher and lower sediment densities, respectively. The glacio-marine, brackish and lacustrine phases correspond to zones 1, 2 and 3, respectively. [Color figure can be viewed at wileyonlinelibrary.com]

Si, K, Ca, Ti, Mn, Fe contents and Mn/Ti were relatively high at the beginning of zone 1 but decreased abruptly at the end of the section. This decreasing trend continued, and values reached their minima by the end of zone 2. They then increased above the 33 cm horizon, marking the onset of zone 3. Ca/Ti values were relatively high during zone 1 and similarly decreased above this unit. However, they decreased substantially above 33 cm, reaching their minimum after this transition.

- Core Fury-2F
While Fury-2F (Fig. 5) was relatively homogeneous, Si, K, Ca, Ti, Mn, Fe and Mn/Ti values increased continuously above 31 cm. Ca/Ti followed an opposite trend.
- Core Fury-2C
Core Fury-2C (Fig. 6) consisted of three significant stratigraphic zones: (1) a bottom organic-poor section (82–57 cm); (2) a transitional mid-section (57–52 cm); and (3) a top organic-rich lacustrine section (52–0 cm). Ca content remained relatively

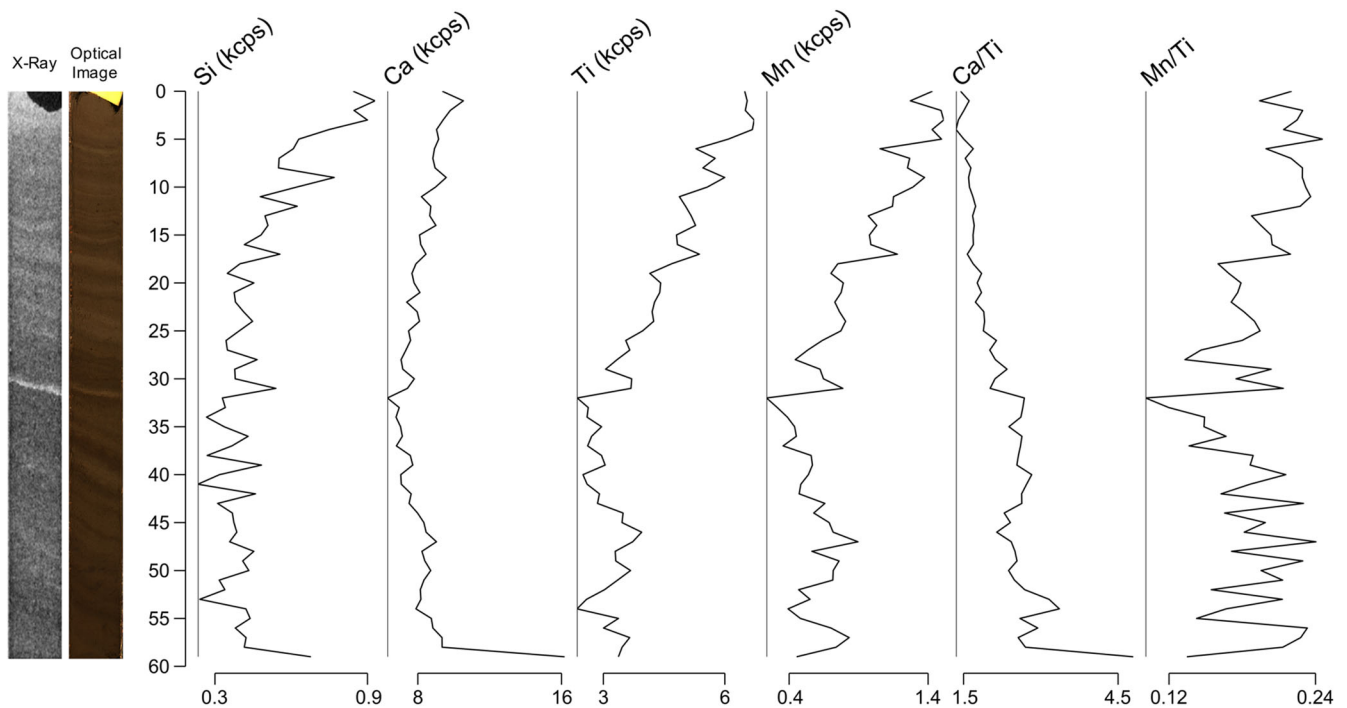


Figure 5. Averaged (i.e. 1 cm averages) geochemical profiles throughout core Fury-2F, only comprising lacustrine organic sediments. [Color figure can be viewed at wileyonlinelibrary.com]

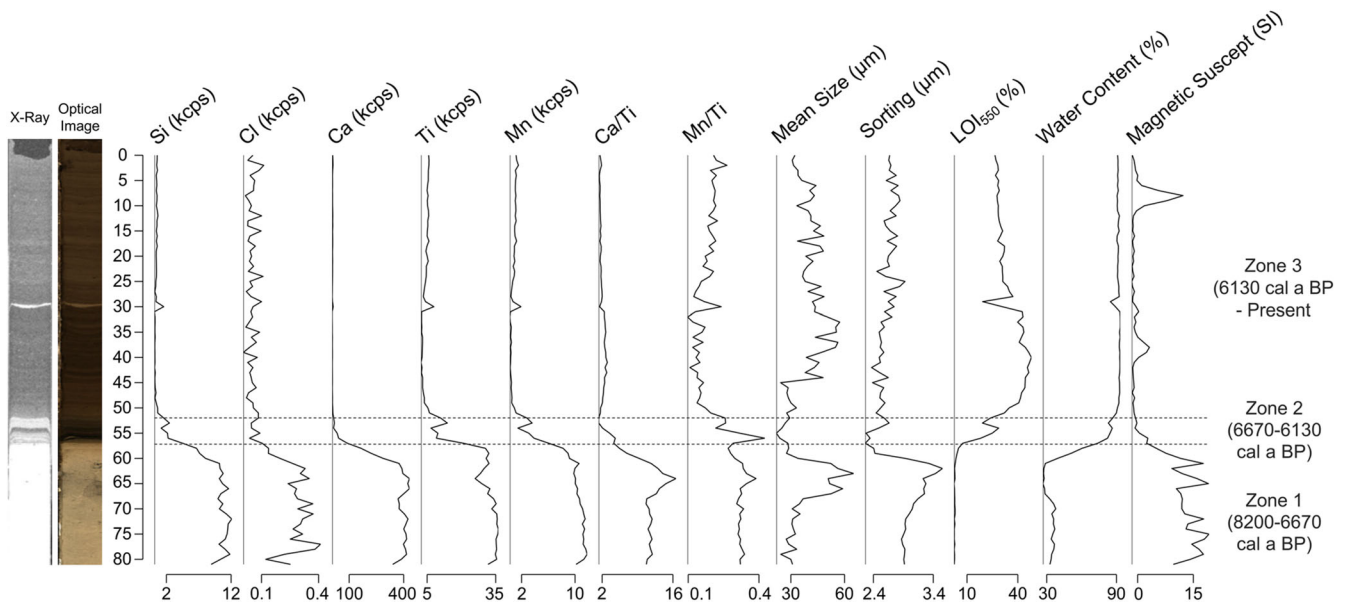


Figure 6. Averaged (i.e. 1 cm averages) geochemical, lithological and sedimentological profiles throughout core Fury-2C. The glacio-marine, brackish and lacustrine phases correspond to zones 1, 2 and 3, respectively. [Color figure can be viewed at wileyonlinelibrary.com]

high during zone 1 but experienced a continuous decrease near the top of this unit, reaching significantly lower values during zone 2. This trend continued and values reached their minimum within zone 3, following the transitional phase. Si, K, Ti, Mn, Fe relative concentrations and Mn/Ti generally reached their highest values during zone 1 and gradually decreased during zone 2. While their minima were reached during the early stages of zone 3, they peaked abruptly at 30 cm, and gradually increased above this layer. Ca/Ti initially followed a similar trajectory, reaching its maximum value in zone 1 and gradually decreasing during zone 2. The ratio then increased at the onset of zone 3. However, contrary to the previous profiles, it reached a local minimum at 30 cm and then gradually decreased upwards.

Grain-size analysis

The sediments of core Fury-2C mainly displayed a bimodal distribution and remained poorly sorted overall, with spread values fluctuating between 2 and 4 µm (Fig. 6). Zone 1 was characterised by relatively high sorting, particularly during its final stages. While the 82–67 cm interval was marked by relatively high sorting (ranging from 2.87 to 3.15 µm, indicating poorly sorted sediments), an important shift towards higher values ranging from 3.25 to 3.55 µm, indicating poorer sorting conditions, occurred between 67 and 63 cm (7690–7370 cal a BP). Values decreased drastically following this interval and reached their minimum (2.26 µm) at 58 cm (6880 cal a BP), marking the beginning of zone 2. Low sorting values remained relatively stable throughout this phase and no significant changes were recorded along zone 1.

Lithology

Organic matter content (LOI₅₅₀) varied from 2%, in the downcore glacio-marine section of Fury-2C, to almost 50% in the upper lacustrine section (Fig. 6). Values remained very low in zone 1 (maximum = 3%) and abruptly increased to 30% in zone 2. This increase continued during the early stages of zone 3, and maximum LOI₅₅₀ values (40% to 50%) were recorded within the 50–30 cm interval (5980–3930 cal a BP) of the unit. However, the ongoing increase ceased above 30 cm,

with LOI₅₅₀ content abruptly dropping to 19%. LOI₅₅₀ values then remained relatively low and did not reach their initial levels in the following interval (29–0 cm), ranging from 26% to 37%.

The same general pattern was observed in water content, which gradually increased (from 25% to 94%) towards the top section, with a slight decrease to 84% at 30 cm depth.

A sustained decrease in MS from 12 to 20 SI (during zone 1) to 0 SI (zones 2 and 3) was also recorded throughout the core (Fig. 6). Low MS values were maintained during zone 3, converging with the previous results. This trend was not affected at 30 cm depth, but prominent peaks were recorded at 39 and 9 cm (ca. 5000 and 1900 cal a BP), respectively.

Principal component analysis

Zone 3 of core Fury-2C (interpreted as the lacustrine phase) was analysed using a PCA (Fig. 7) to better visualise and investigate environmental shifts experienced during the basin's final stage (last ~6100 years). The first two axes explained 80.71% of the total variance in the standardised dataset; the first and second axes, respectively, accounted for 67.26 and 13.45%. All variables were well represented on the principal components (Table 3) and grouped into two main categories, namely (1) a cluster associated with detrital inputs (Si, Ca, K, Ti, Mn, Fe), and (2) a cluster associated with water content and LOI₅₅₀. The first cluster was positively correlated with axis 1 while the second, biomass-related cluster was negatively correlated with it. It is noteworthy that Ca/Ti and Mn/Ti (supplementary variables) were strongly positively and negatively correlated with LOI₅₅₀, respectively. Axis 2 was positively correlated with mean grain-size, sorting and MS values. Furthermore, the PCA (Fig. 8) separated the samples into two groups along axis 1.

Diatoms

Diatom frustules were generally well preserved and consisted of 33 genera comprising 121 species, 20 of which were then selected (>5% relative abundance in at least one sample) and classified according to their salinity (halobian) tolerances based on Campeau et al. (1999) (Fig. 9). Samples below 65 cm depth were excluded from the analyses due to

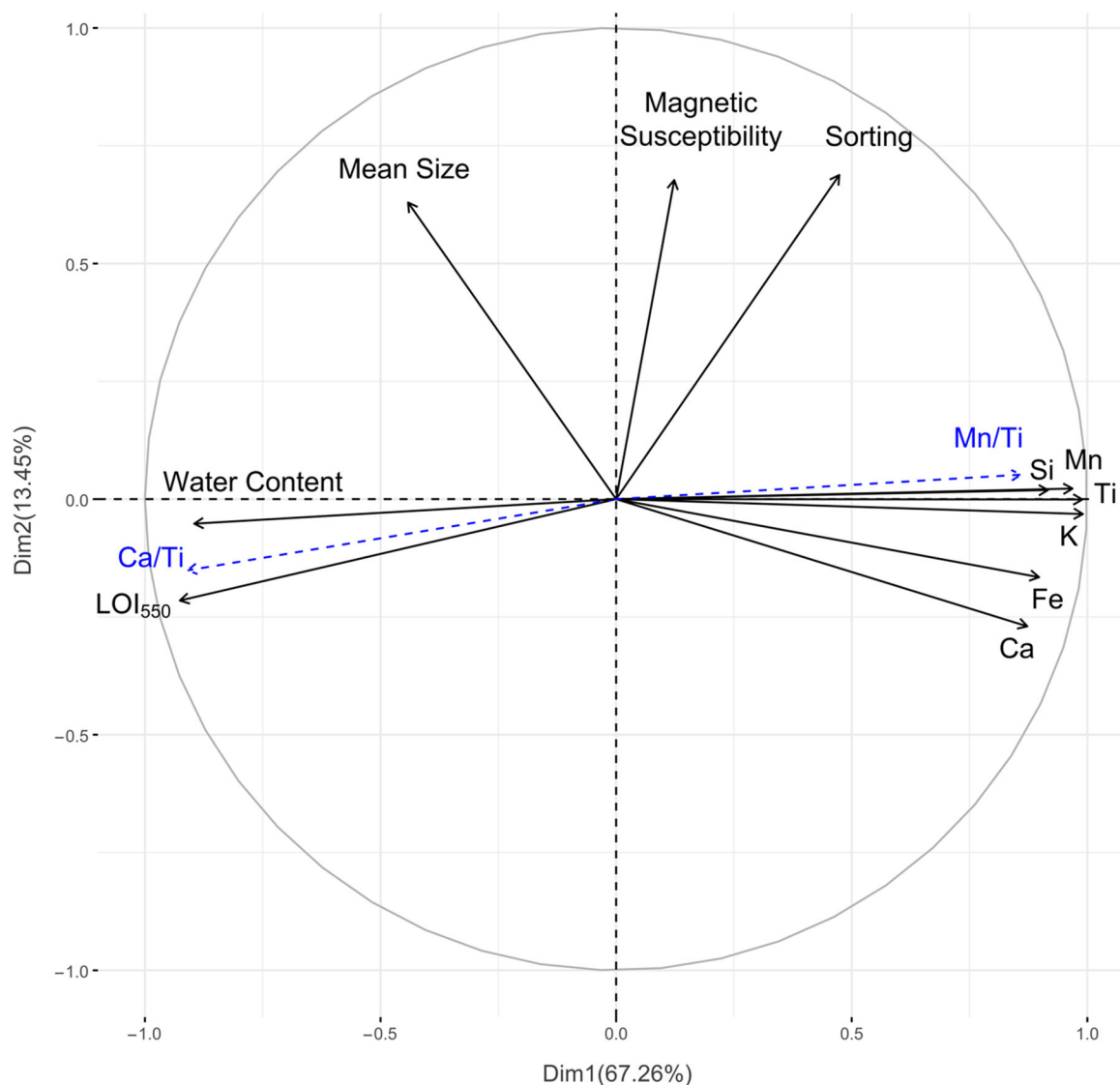


Figure 7. Two-dimensional plot of the variables on the principal component analysis (PCA) ordination (axes 1 and 2) computed for all 11 standardised environmental variables measured in the lacustrine section (zone 3) of core Fury-2C (last ~6100 years). The circle of radius 1 represents the maximum length (contribution) for a vector in the PCA. Ca/Ti and Mn/Ti (blue arrows) were included only as supplementary variables. [Color figure can be viewed at [wileyonlinelibrary.com](https://onlinelibrary.com)]

extremely low valve concentrations. Taxa were categorised into four groups: polyhalobian (20 ppt–35 ppt), mesohalobian (0.2 ppt–30 ppt), oligohalobian (indifferent taxa) and halophobian (freshwater taxa) (Campeau et al., 1999; Narancic et al., 2016). Although the subfossil floras were generally dominated by fragilarioid taxa (e.g. *Staurosirella pinnata* and *Staurosira venter*) common in small Arctic lakes (Pienitz et al., 1995; Adams and Finkelstein, 2010), notable changes were observed throughout the core and there were four significant diatom zones (DZ). Three were similar to those in the XRF dataset, namely the glacio-marine (DZ1), brackish (DZ2) and lacustrine (DZ3) zones. The algorithm separated the lacustrine phase into two distinct groups based on taxonomic differences, and DZ3 was therefore subdivided into two subzones: DZ3a and DZ3b.

- DZ1 (7600–6670 cal a BP; 65–57 cm)
Characterised by the dominance of salinity-tolerant taxa typical of marine/brackish environments, which mainly consisted of *Thalassiosira baltica* (reaching a maximum relative abundance of 32%), *Diploneis smithii* (20%), *Cocconeis costata* (9%), *Trachyneis aspera* (8%), *Bacillaria socialis* (7%), *Pinnularia quadratarea* (6%), *Navicula directa*

(6%) and *Tabularia fasciculata* (5%). While oligohalobian pioneer fragilarioid species dominated by *Staurosirella pinnata* (24%), *Pseudostaurosira pseudoconstruens* (18%) and *Pseudostaurosira brevistriata* (6%) were also present, their minimum relative abundances were reached within this phase. The $\exp(H)$ index indicated relatively rich and diverse diatom communities, with values ranging from 8.83 to 17.57.

- DZ2 (6670–6130 cal a BP; 57–52 cm)
DZ2 was marked by an abrupt decline and disappearance of polyhalobian species, with the exception of *D. smithii* (commonly described as a brackish–marine taxon found in shallow littoral zones; Leland et al., 1995), accompanied by an increase of *S. pinnata*, *P. brevistriata* and *P. pseudoconstruens*, the latter two showing their highest occurrences during this phase (23% and 52%, respectively). This zone was also marked by the initial appearance of the oligohalobian *Staurosira venter*, as well as the mesohalobian *Cyclostephanos dubius* (reaching a relative abundance of 23%). These important compositional changes were also accompanied by a gradual decrease in diversity, with values dropping from 10.88 to 4.29.

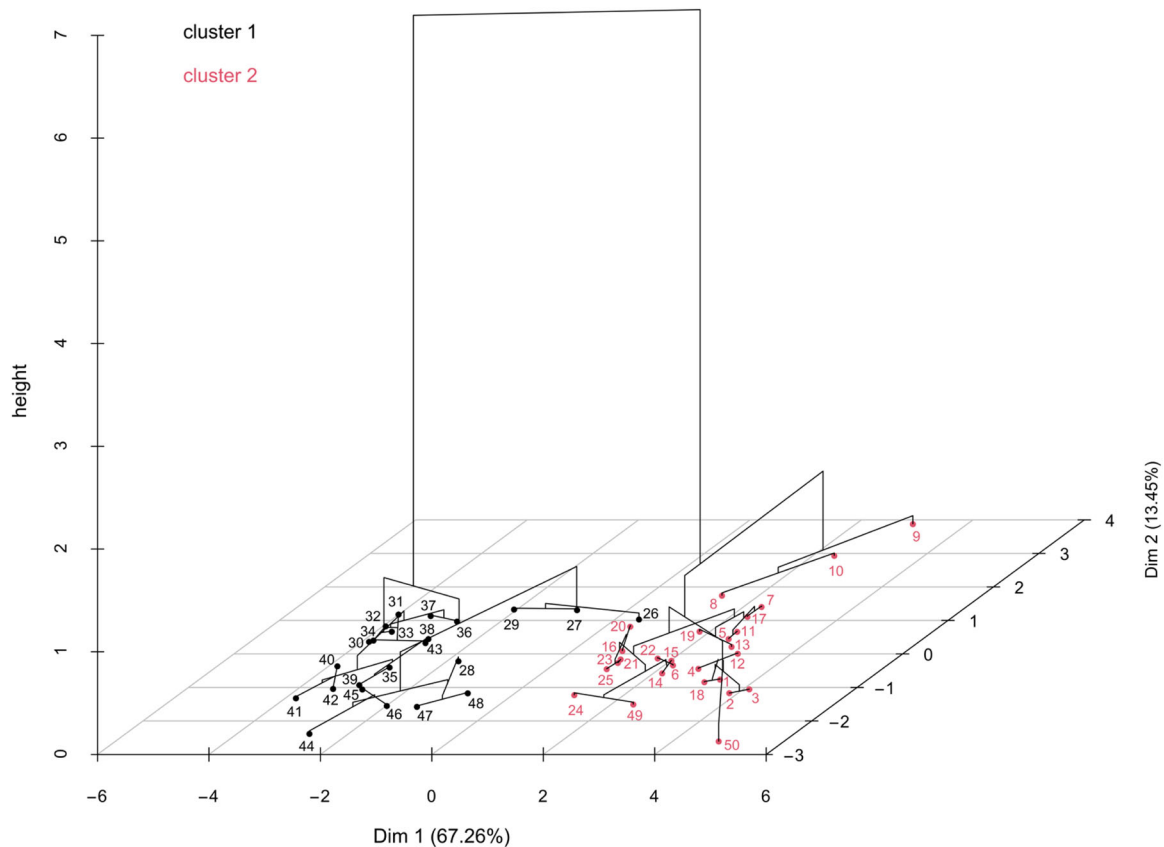


Figure 8. Hierarchical clustering of all 50 observations in the lacustrine section (zone 3) of core Fury-2C (with the exception of the outliers at 29 and 30 cm) and their distribution on the PCA ordination. Samples of the lower lacustrine section form a black cluster (left) associated with negative PCA scores, while those of the upper lacustrine section form a second, red cluster (right) associated with positive scores. [Color figure can be viewed at wileyonlinelibrary.com]

- DZ3 (6130 cal a BP – present; 52–0 cm)

Salinity-tolerant taxa disappeared at the onset of DZ3 and freshwater taxa became dominant, including oligohalobian and halophobian species. Diatom assemblages changed significantly at the 25 cm horizon, thus dividing DZ3 into two distinct subzones (DZ3a and DZ3b).

- a. DZ3a (ca. 6130–3630 cal a BP; 52–25 cm)

Diversity continued to decrease at the beginning of DZ3a, eventually reaching its lowest value (3.51). Small tycho-planktonic fragilarioids, including *P. pseudoconstruens*, *P. brevistriata*, *S. venter* and *S. pinnata* (dominant taxon), most of which reached their highest frequency at that time, attained a combined maximum relative abundance of ~90% during the subzone's early stages. Subsequently, several oligohalobian and halophobian species, dominated by *Karayevia suchlandtii*, *Amphora pediculus*, *Lindavia bodanica* and *Planothidium oestrupii*, progressively appeared, resulting in an important increase in diversity from 40 cm (ca. 5000 cal a BP) upward.

- b. DZ3B (3630 cal a BP – present; 25–0 cm)

This subzone was marked by a gradual decrease in the dominant fragilarioid taxa, the establishment of halophobian species, mostly dominated by *Cocconeis placentula* and *Karayevia laterostrata*, as well as the disappearance of *Platessa conspicua*. Diversity continued to increase during this stage but reached relatively stable values fluctuating between 7.58 and 11.54 from 22 cm upward (3500 cal a BP – present).

Species–environment relationships

According to the global test, the RDA (Fig. 10) performed with all explanatory variables (recorded during the lacustrine phase

of core Fury-2C) was significant ($P=0.001$). A total of three significant environmental variables were then selected based on their Bonferroni-corrected P values obtained by forward selection, namely LOI_{550} , K and mean July western Arctic Holocene temperatures ($P=0.0001$, 0.0001 and 0.009 and adjusted $R^2=0.47$, 0.08 and 0.03 , respectively). The two first canonical axes explained 48.44% of the overall variance observed in the response matrix (39.31% and 9.13%, respectively). LOI_{550} and western Arctic mean July temperatures displayed a strong positive correlation with RDA1 ($R=0.95$ and 0.85 , respectively), whereas K showed a negative correlation with this axis ($R=-0.77$). Species such as *Staurosirella pinnata* and *Platessa conspicua* appeared to be influenced by mean July temperatures and LOI_{550} , while *Lindavia bodanica*, *Cocconeis placentula* and *Karayevia laterostrata* were negatively correlated with the latter two variables.

The most informative predictors selected by the MRT (Fig. 11) were LOI_{550} , western Arctic mean July temperatures and Mn. The model divided the 50 samples into five distinct groups, based on the lowest computed CVRE value (0.67), with an R^2 of 0.67. Although these groups were similar in terms of species composition (presence–absence), prominent changes were obvious, and the five leaves were clustered into two distinct categories: those with diatom assemblages associated with potentially warm conditions versus those with colder conditions. The main LOI_{550} -controlled data split was done according to a threshold of 32.09%, and secondary splits were controlled by western Arctic mean July temperatures and Mn relative concentrations, with threshold values of 6.8°C and 1.01 kcps, respectively. The first group was characterised by the dominance of a few pioneer species, including *S. pinnata*

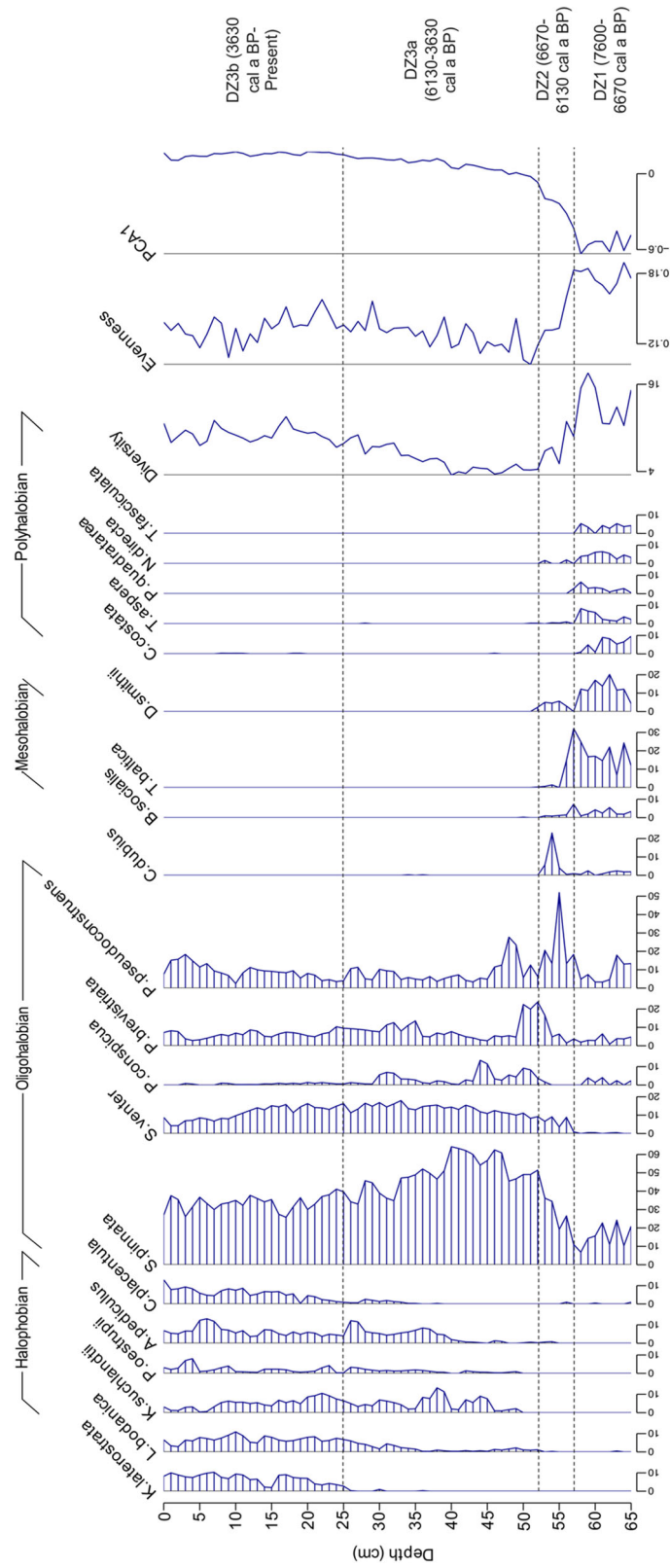


Figure 9. Relative abundances of the major diatom taxa (>5% in at least one sample), grouped according to their salinity tolerances, in addition to alpha diversity, evenness and PCA axis 1 sample scores throughout core Fury-2C. All significant diatom zones are presented at the right of the figure. [Color figure can be viewed at wileyonlinelibrary.com]

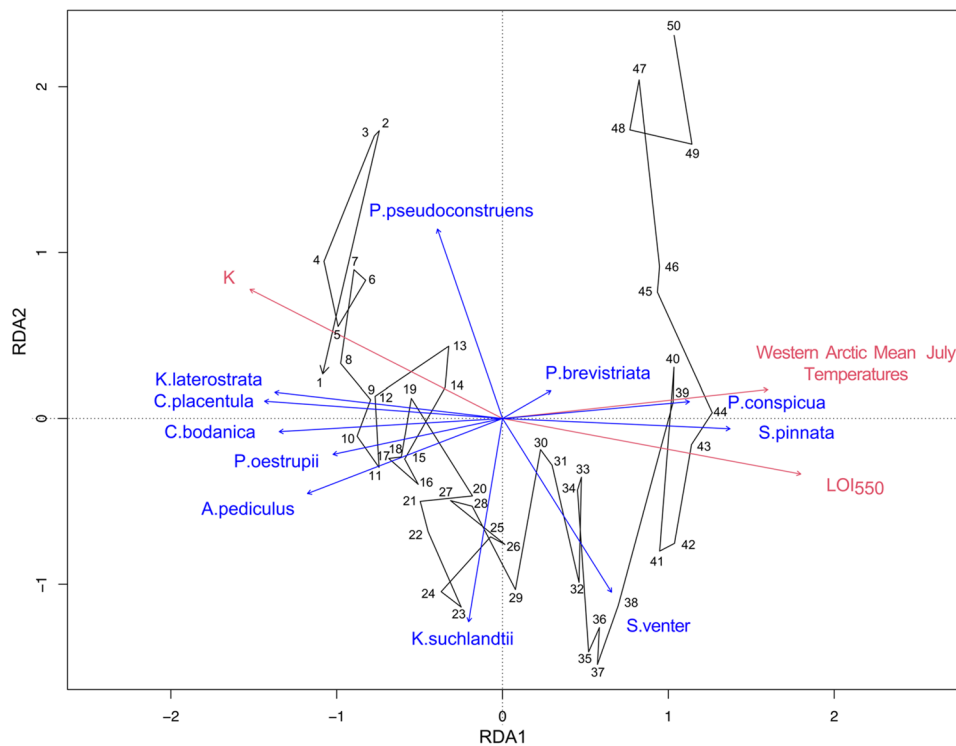


Figure 10. Redundancy analysis (RDA) triplot showing the statistically significant environmental variables (red arrows), the 11 major diatom taxa (blue arrows) and the 50 observations in the lacustrine section (zone 3) of core Fury-2C, distributed along the first two canonical axes. Time-series trajectory is represented by the arrow connecting all samples from 50 (bottom) to 1 (surface). [Color figure can be viewed at wileyonlinelibrary.com]

and *S. venter* and an overall low diversity, while the second group was marked by a significant decrease in species such as *P. conspicua*, the establishment of *C. placentula* and *K. laterostrata*, as well as a net increase in diversity and evenness.

Discussion

Significant shifts in the geochemical, sedimentological and diatom profiles from cores Fury-1 and Fury-2C suggest major Holocene palaeogeographical and palaeohydrological changes, namely the beginning of deglaciation and marine inundation. In addition, core Fury-2C potentially records climatic fluctuations (based on LOI₅₅₀ and Ca/Ti profiles) from the mid-Holocene onward (~6000 cal a BP – present).

Glacio-marine phase

The glacio-marine sediments identified in cores Fury-1 and Fury-2C accumulated during a period of isostatic subsidence (Narancic et al., 2016). Highly fluctuating Cl, Ti, Mn, Fe and grain-size values in both cores (as well as MS values in core Fury-2C; Figs. 4 and 6) likely originate from the gradual breakup of the Foxe Ice Dome, which led to rapid glacial outwash and marine inundation (Narancic et al., 2016). This is confirmed by high Ca and K values, also characteristic of marine conditions (Rolland et al., 2008). Nonetheless, while the presence of polyhalobian taxa such as *D. smithii*, *C. costata*, *N. directa*, *T. fasciculata*, *T. aspera* and *P. quadratarea* points towards a saline environment (Fig. 9), the predominance of the mesohalobian species *T. baltica* suggests that glacial meltwaters prevented the establishment of fully marine conditions, creating a highly variable brackish environment through mixing and dilution processes (Campeau et al., 1999). Moreover, the benthic and epiphytic nature of *C. costata* indicates relatively shallow nearshore

waters (Al-Handal and Wulff, 2008; Majewska et al., 2016). Several diatom frustules were fragmented in this bottom section, suggestive of highly dynamic conditions in the context of deglaciation (Pienitz et al., 1991; Adams and Finkelstein, 2010).

Similarly, increases in LOI₅₅₀ and Ca/Ti in Fury-1 and Fury-2C (Figs. 4 and 6) possibly suggest higher biomass production during this phase, likely due to rising summer temperatures and longer open water seasons during the Holocene thermal maximum (Narancic et al., 2016). This is substantiated by the presence of glacial dropstones in Fury-2C, in addition to an important number of bryophyte remains in Fury-1, requiring increasingly ice-free conditions due to their poikilohydric nature (Singh et al., 2018). This, however, should be carefully interpreted, as higher organic matter content can also be explained by periods of increased anoxia that favour organic carbon burial (Sobek et al., 2009).

Our age–depth model yields a deglaciation age of ~8200 cal a BP at the latest, as inferred from the oldest dated bryophyte fragments extracted from core Fury-2C. At that time, the marine gateway and connection between the waters of the Atlantic and Pacific oceans arriving from Foxe Basin and the Gulf of Boothia must have been established. Dredge (2001) suggested that the strait was deglaciated after 7750 cal a BP (obtained by calibrating Dredge's ¹⁴C age, i.e. 6900 ¹⁴C a BP), when the ice broke up in Foxe Basin, while Dyke (2008) suggested that the process was operating from 9500 cal a BP (8500 ¹⁴C a BP) until somewhat after 7400 cal a BP (6500 ¹⁴C a BP). However, our results inferred from Fury-1 and Fury-2C provide a more precise timing of local events and indicate that regional deglaciation was likely complete at least ~800 years earlier than previously suggested. These conclusions converge with the model of Narancic et al. (2016) who argued that marine inundation was initiated at least 8300 cal a BP in southeastern Foxe Basin, as recorded from Nettilling Lake sediments. It is noteworthy that the catchment bedrock and surficial deposits of our study lakes were devoid of carbonates

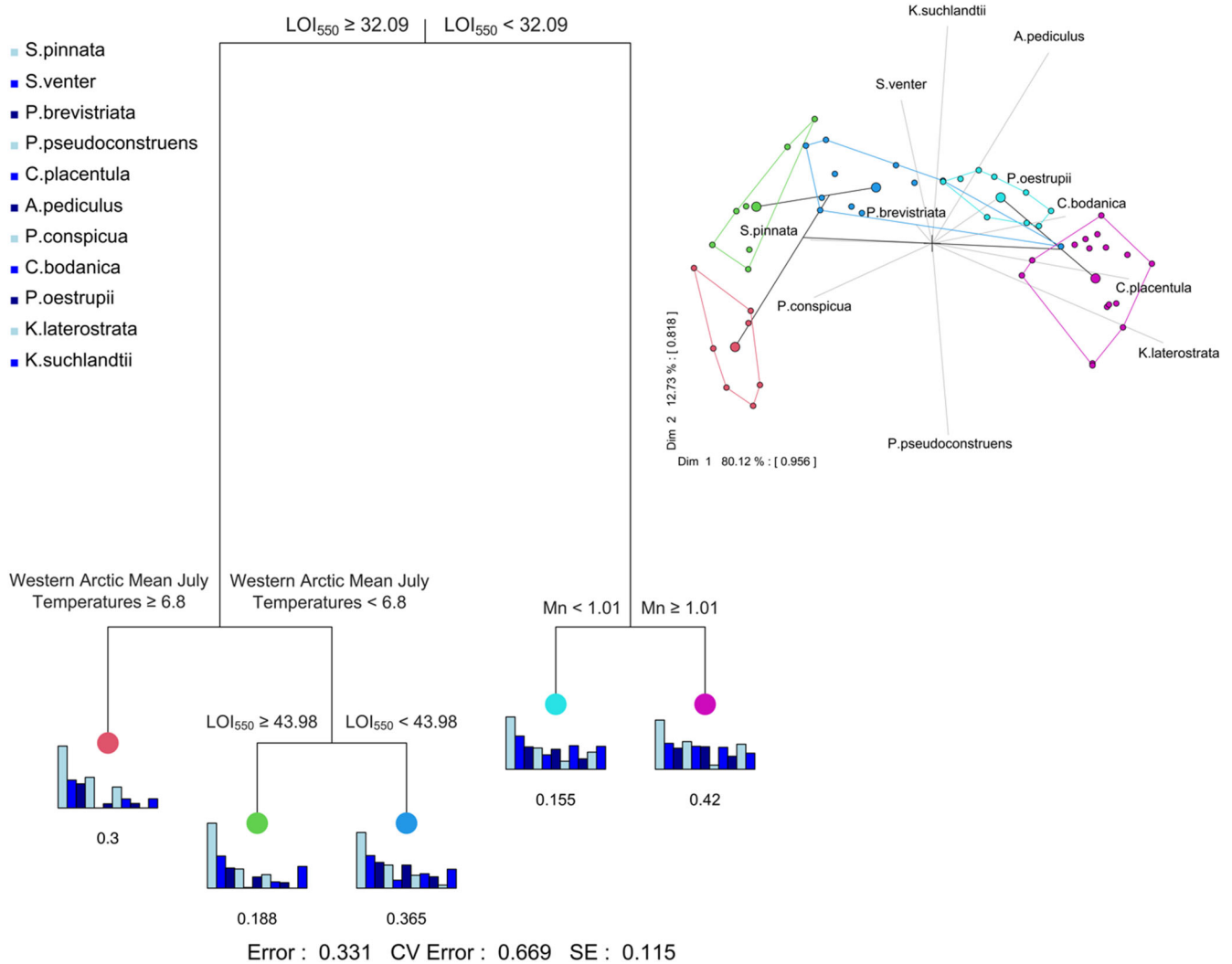


Figure 11. Multivariate regression tree modelling the relationship between the most predictive environmental variables and the major diatom taxa. The bar plots represent the 11 species, running from left to right at the end of each leaf. The relative lengths of the branches are proportional to the total sum of squares explained by each split, and each assemblage is associated with a coloured dot referring to a cluster in the PCA ordination (upper right). The colours correspond to groups of core slices that are fairly homogeneous in diatom composition. The largest dots in the PCA ordination represent the cluster centroids. [Color figure can be viewed at wileyonlinelibrary.com]

and glacial meltwater inputs which could have otherwise affected the radiocarbon ages.

Marine regression and basin isolation

Glacial isostatic adjustment was well underway during the glacio-marine phase and gradually isolated the regional basins from marine influence. Lake Fury 1 may have been rapidly isolated from the postglacial sea due to its higher threshold elevation (204 m asl). This was reflected in the sharp nature of its isolation contact, as indicated by a sudden drop in Ca, K and Cl activities ca. 8100 cal a BP, shortly after marine transgression (Fig. 4). Moreover, this observation suggests that the postglacial marine limit could possibly have been much higher (≥ 85 m asl) than previously reported by Dredge (1991, 2001) for northeastern Melville Peninsula. However, this site was located in a zone of important westward glacial dispersal across Palaeozoic carbonate rocks, where ice streams originating from Foxe Basin were transporting regional marine sediments (Dredge, 2000). The latter could have potentially redeposited at the bottom of Lake Fury 1, therefore explaining the presence of a glacio-marine sequence well above the marine limit elevation previously determined based on raised beaches (Dredge, 1991).

On the other hand, a gradual and sustained decrease in Cl, K, Ca, LOI_{550} and MS values following the isolation contact indicates a more gradual and stepwise isolation of Lake Fury 2 around 6670 cal a BP (Fig. 6). These observations mark the beginning of the brackish phase and are supported by the disappearance of all polyhalobian taxa and the emergence of mesohalobian taxa dominated by *C. dubius*, typical of brackish environments and nutrient-rich conditions (Bradshaw and Anderson, 2003; Houk et al., 2014) (Fig. 9). Furthermore, a gradual and consistent increase in tycho planktonic oligohalobian fragilarioids suggests the establishment of a shallow and highly dynamic environment (Pienitz et al., 1991; Campeau et al., 1999). This basin remained under brackish influence for a relatively short period (until ca. 6130 cal a BP), likely due to its smaller ratio of lake surface to drainage basin area, in addition to its shallower nature, thereby allowing increased freshwater runoff and accelerated bottom-water renewal (Pienitz et al., 1991).

Lacustrine phase

Lake Fury 1

The onset of the lacustrine phase was punctuated by a rapid shift of lithological and geochemical properties in core Fury-1,

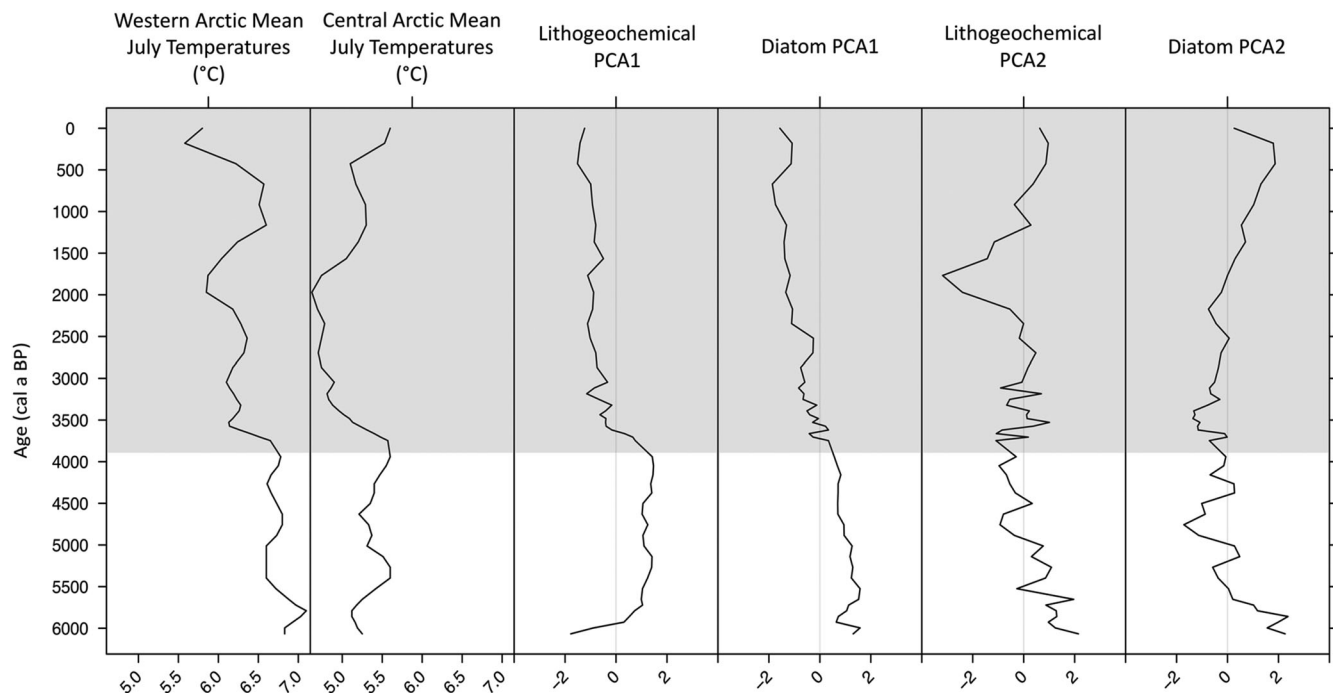


Figure 12. Synthesis of the lithochemical and biostratigraphic data of the lacustrine section of core Fury-2C (zone 3). PCA axes 1 and 2 scores of both datasets are plotted against age and compared with pollen-inferred Holocene temperatures reconstructed by Gajewski (2015). The shaded area marks a shift in both the PCA scores and regional palaeotemperatures around 3900 cal a BP. Lower values in lithochemical and diatom PCA axis 1 scores are generally associated with colder temperatures.

and possibly lower biomass accumulation inferred from a slight decrease in the Ca/Ti ratio (Fig. 4). This was further substantiated by increasing Mn/Ti values, hinting at higher oxygenation of the water column (Schilder et al., 2017). Indeed, a decrease in primary productivity increases dissolved oxygen availability which would otherwise be impeded by bacterial respiration during warmer periods of high productivity (Loizeau et al., 2001; Wetzel, 2001; Davies et al., 2015).

Lake Fury 2

Diatom assemblages

The presence of benthic species such as *K. suchlandtii*, *K. laterostrata* and *C. placentula* (in addition to the above-mentioned fragilarioid taxa) punctuating DZ3 suggests a shallow basin with high light penetration and relatively low dissolved nutrient concentrations throughout this interval. Furthermore, the establishment of *P. conspicua* and *K. laterostrata* during DZ3a and DZ3b indicates circumneutral pH during the entire lacustrine phase (Szabó et al., 2017; Brown et al., 2019).

Multivariate analyses

The PCA ordination (Fig. 7) shows that detrital inputs were positively correlated with axis 1, while LOI₅₅₀ was negatively correlated with this axis. Given the high contribution of these variables to axis 1 (and the strong positive correlation between Ca/Ti and LOI₅₅₀), we conclude that this component likely follows a temperature/biomass gradient from negative (warmer and relatively productive conditions) to positive scores (colder conditions). Fig. 8 therefore potentially reflects a shift from warmer to colder conditions, indicating that the regional climate remained relatively warm until ~3900 cal a BP, before the onset of a prolonged cooling episode (Fig. 6). However, as previously mentioned, this may also be related to enhanced organic matter preservation (Sobek et al., 2009) and should therefore be interpreted with caution. Nevertheless, this

pattern is well documented and observed in several lake sediment cores from Baffin Island, most of which record significant glacial readvances and the onset of Neoglaciation after ~3500 cal a BP (Briner et al., 2009). Several other palaeolimnological studies conducted in the Canadian Arctic Archipelago (e.g. Finkelstein and Gajewski, 2008) also confirm this hypothesis by noting a significant cooling trend that intensified following 4000 cal a BP.

Likewise, RDA (Fig. 10) indicated that the variance in the diatom dataset was mainly driven by changes in LOI₅₅₀ (potentially mediated by temperature) and western Arctic mean July temperature fluctuations during the Holocene (Gajewski, 2015). The MRT (Fig. 11) also suggested that this variation is best explained by changes in organic matter content (in conjunction with western Arctic temperatures and Mn), where splits partitioned the response matrix into two major clusters possibly associated with colder and warmer conditions.

Our results suggest that biological communities of Lake Fury 2 responded to the same palaeoclimatic trajectory, both directly to variations in regional temperatures and indirectly to changes in organic matter accumulation. General variations in the lithochemical and biological datasets of zone 3 of core Fury-2C reflect this trajectory, as changes in the PCA scores of both proxy groups are consistent with palaeoclimatic shifts (Fig. 12). Given that core Fury-1 shows the same pattern (Fig. 4), and assuming similar sedimentation rates in both lakes, we propose that this long-term cooling trend is of regional nature.

Conclusions

We reconstructed the palaeoenvironmental and palaeoclimatic evolution of the Fury and Hecla Strait region since deglaciation, including ecological, hydrological and geomorphological changes. From this multiproxy approach, which combined micropalaeontological, sedimentological and geochemical tools, we draw the following conclusions:

- Climate warming triggered the gradual breakup of the Foxe Ice Dome, leading to a rapid regional marine inundation and glacial meltwater input, 8200 cal a BP at the latest. This is reflected through a glacio-marine phase, characterised by the dominance of marine polyhalobian and mesohalobian diatom taxa, as well as rapidly fluctuating detrital inputs, grain-size and magnetic susceptibility values.
- The oldest ¹⁴C-dated bryophyte fragments from core Fury-2C suggest a glacio-marine phase that started ~8200 cal a BP at the latest. This yields an age for regional deglaciation at least ca. 800 years earlier than previously calculated by extrapolation. By that time, the connection between the Atlantic and Pacific waters must have been established.
- Following the retreat of the Laurentide Ice Sheet, glacial isostatic adjustment was well underway, leading to the emergence and gradual isolation from marine influence of regional basins. Lake Fury 1 (204 m asl) was isolated promptly after deglaciation (8100 cal a BP) due to its high threshold elevation, while Lake Fury 2 (65 m asl) was isolated about 6670 cal a BP.
- The regional climate may have remained relatively warm until ~3900 cal a BP. This horizon is marked by important lithological changes in cores Fury-2F and Fury-2C, followed by a prolonged cooling interval possibly ascribed to the Neoglacial, as inferred from an important decrease in biomass accumulation. Multivariate analyses further support this hypothesis by showing that changes in diatom assemblages were mainly driven by a similar shift. Moreover, geochemical changes recorded in core Fury-1 confirm the regional nature of this cooling episode. These findings converge with the regional trend reported in previous studies.

Acknowledgements. This study was funded through Discovery (04743-2017) and Northern Research Supplement (305489-2017) grants awarded to R. Pienitz from the Natural Sciences and Engineering Research Council (NSERC) of Canada. Logistic support was provided by the Polar Continental Shelf Program (PCSP), the Northern Scientific Training Program (NSTP) and the Centre d'études nordiques (CEN), Université Laval. We thank A. De Coninck and P. Francus (INRS-ETE) for geochemical analyses, as well as D. Muir and X. Wang (Environment Canada, Burlington, Ontario) for water chemistry analyses. We are grateful to A. Dyke for his constructive comments on the manuscript. We would also like to thank all members of the Aquatic Paleoecology Laboratory (LPA) for inspiring fruitful and stimulating discussions, as well as K. Bywater-Brenna and I. El Haddaoui for assistance in the field. Finally, the authors wish to thank A.W. Mackay and one anonymous reviewer for their valuable comments. The authors declare no conflicts of interest.

Data availability statement

The data that support the findings of this study are available on request from the corresponding author.

References

- Adams JK, Finkelstein SA. 2010. Watershed-scale reconstruction of middle and late Holocene palaeoenvironmental changes on Melville Peninsula, Nunavut, Canada. *Quaternary Science Reviews* **29**: 2302–2314.
- Al-Handal AY, Wulff A. 2008. Marine benthic diatoms from Potter Cove, King George Island, Antarctica. *Botanica Marina* **51**: 51–68.
- Antoniades DA, Hamilton PB, Douglas MSV *et al.* 2008. Diatoms of North America: the freshwater floras of Prince Patrick, Ellef Ringnes and northern Ellesmere Islands from the Canadian Arctic Archipelago. *Iconographia Diatomologica* **17**: 1–649.
- Blaauw M, Christen JA. 2011. Flexible paleoclimate age-depth models using an autoregressive gamma process. *Bayesian Analysis* **6**: 457–474.
- Blaauw M, Christen JA. 2019. rbacon: Age-depth modelling using Bayesian statistics. R package version 2.3.9.1. <https://cran.r-project.org/web/packages/rbacon/index.html>
- Blott SJ, Pye K. 2001. GRADISTAT: a grain size distribution and statistics package for the analysis of unconsolidated sediments. *Earth Surface Processes and Landforms* **26**: 1237–1248.
- Borcard D, Gillet F, Legendre P. 2011. *Numerical Ecology with R. Use R! series*. Springer Science: New York.
- Bradshaw EG, Anderson NJ. 2003. Environmental factors that control the abundance of *cyclostephanos dubius* (bacillariophyceae) in danish lakes, from seasonal to century scale. *European Journal of Phycology* **38**: 265–276.
- Briner JP, Davis PT, Miller GH. 2009. Latest Pleistocene and Holocene glaciation of Baffin Island, Arctic Canada: key patterns and chronologies. *Quaternary Science Reviews* **28**: 2075–2087.
- Brown SR, Fritz SC, Morgan LA *et al.* 2019. Fossilized diatoms of siliceous hydrothermal deposits in Yellowstone National Park, USA. *Diatom Research* **34**: 193–204.
- Campeau S, Pienitz R, Héquette A. 1999. Diatoms from the Beaufort Sea Coast, southern Arctic-Ocean (Canada). Modern analogues for reconstructing Late Quaternary environments and relative sea levels. *Bibliotheca Diatomologica* **42**: 1–244.
- Coad BW, Reist JD. 2018. *Marine Fishes of Arctic Canada*. University of Toronto Press: Toronto.
- Croudace IW, Rindby A, Rothwell RG. 2006. ITRAX: description and evaluation of a new multi-function X-ray core scanner. In *New Techniques in Sediment Core Analysis*, R. Rothwell G (ed). Geological Society of London: London; 51–63.
- Cuven S, Francus P, Lamoureux S. 2011. Mid to Late Holocene hydroclimatic and geochemical records from the varved sediments of East Lake, Cape Bounty, Canadian High Arctic. *Quaternary Science Reviews* **30**: 2651–2665.
- Davies SJ, Lamb HF, Roberts SJ. 2015. Micro-XRF core scanning in palaeolimnology: recent developments. In *Micro-XRF Studies of Sediment Cores*, Croudace IW, Rothwell RG (eds). Springer: Berlin; 189–226.
- De'ath G. 2002. Multivariate regression trees: A new technique for modeling species-environment relationships. *Ecology* **83**: 1105–1117.
- Dredge LA. 1990. The Melville Moraine: sea-level change and response of the western margin of the Foxe Ice Dome, Melville Peninsula, Northwest Territories. *Canadian Journal of Earth Sciences* **27**: 1215–1224.
- Dredge LA. 1991. Raised Marine Features, Radiocarbon Dates, and Sea Level Changes, Eastern Melville Peninsula. *Arctic Canada*. *Arctic* **44**: 63–73.
- Dredge LA. 2000. Carbonate dispersal trains, secondary till plumes, and ice streams in the west Foxe Sector, Laurentide Ice Sheet. *Boreas* **29**: 144–156.
- Dredge LA. 2001. Late Pleistocene and Holocene glaciation and deglaciation of Melville Peninsula, northern Laurentide Ice Sheet. *Géographie Physique et Quaternaire* **55**: 159–170.
- Dyke AS. 2004. An outline of North American deglaciation with emphasis on central and northern Canada. In *Quaternary Glaciations-Extent and Chronology, Part II*, Ehlers J, Gibbard PL (eds). Elsevier: New York; 373–424.
- Dyke AS. 2008. The Steensby Inlet Ice Stream in the context of the deglaciation of Northern Baffin Island, Eastern Arctic Canada. *Earth Surface Processes and Landforms* **33**: 573–592.
- Dyke AS, Hooper J, Savelle JM. 1996. A history of sea ice in the Canadian Arctic archipelago based on postglacial remains of the bowhead whale (*Balaena mysticetus*). *Arctic* **49**: 235–255.
- Dyke AS, Prest VK. 1987. Late Wisconsinan and Holocene History of the Laurentide Ice Sheet. *Géographie physique et Quaternaire* **41**: 237–263.
- Dyke AS, Savelle JM, Johnson DS. 2011. Paleoeskimo Demography and Holocene Sea-level History, Gulf of Boothia, Arctic Canada. *Arctic* **64**: 151–168.

- Environment Canada (2019). Climate Normals. Available online at http://climate.weather.gc.ca/climate_normals. Accessed June 28, 2019.
- Fallu M-A, Allaire N, Pienitz R. 2000. Freshwater diatoms from northern Québec and Labrador (Canada). Species-environment relationships in lakes of boreal forest, forest-tundra and tundra regions. *Bibliotheca Diatomologica* **45**: 1–200.
- Finkelstein SA, Gajewski K. 2008. Responses of Fragilarioid-dominated diatom assemblages in a small Arctic lake to Holocene climatic changes, Russell Island, Nunavut, Canada. *Journal of Paleolimnology* **40**: 1079–1095.
- Gajewski K. 2015. Quantitative reconstruction of Holocene temperatures across the Canadian Arctic and Greenland. *Global and Planetary Change* **128**: 14–23.
- Heiri O, Lotter AF, Lemcke G. 2001. Loss on ignition as a method for estimating organic and carbonate content in sediments: Reproducibility and comparability of results. *Journal of Paleolimnology* **25**: 101–110.
- Houk V, Klee R, Tanaka H. 2014. Atlas of freshwater centric diatoms with a brief key and descriptions. Part IV. Stephanodiscaceae B. Stephanodiscus, Cyclostephanos, Pliocenicus, Hemistephanos, Stephanocostis, Mesodictyon & Spicaticribr. *Fottea* **14**: 1–532.
- Husson F, Josse J, Le S *et al.* 2019. FactoMineR: Multivariate Exploratory Data Analysis and Data Mining. R package version 1.42. <https://cran.r-project.org/web/packages/FactoMineR/index.html>
- Ives JD, Andrews JT. 1963. Studies in the physical geography of north central Baffin Island. *Geographical Bulletin* **19**: 5–48.
- Juggins S. 2019. rioja: Analysis of Quaternary Science Data. R package version 0.9-21. <https://cran.r-project.org/web/packages/rioja/index.html>
- Kanamaru K, Francus P, François R *et al.* 2013. New insight into Saanich Inlet varved sediments (British Columbia, Canada) from micro-scale analysis of sedimentary facies and micro-XRF core scanning analyses. *GFF* **135**: 316–339.
- Krammer K, Lange-Bertalot H. 1991a. Bacillariophyceae 3. In *Teil Centrales, Fragilariaceae, Eunotiaceae*, Ettl H, Gärtner G, Gerloff J, Heynig H, Mollenhauer D (eds). Gustav Fischer Verlag: Berlin.
- Krammer K, Lange-Bertalot H. 1991b. Bacillariophyceae 4. In *Teil Achnanthaceae Kritische Ergänzungen zu Navicula (Lineolatae) und Gomphonema*, Ettl H, Grtner G, Gerloff J, Heynig H, Mollenhauer D (eds). Gustav Fischer Verlag: Berlin.
- Kylander ME, Klaminder J, Wohlfarth B *et al.* 2013. Geochemical responses to paleoclimatic changes in southern Sweden since the late glacial: the Hässeldala Port lake sediment record. *Journal of Paleolimnology* **50**: 57–70.
- Larsen DR, Speckman PL. 2004. Multivariate regression trees for analysis of abundance data. *Biometrics* **60**: 543–549.
- Legendre P, Gallagher ED. 2001. Ecologically meaningful transformations for ordination of species data. *Oecologia* **129**: 271–280.
- Legendre P, Legendre L. 2012. *Numerical Ecology*. Elsevier Science: Amsterdam.
- Lepland A, Miller U, Sakson M. 1995. Palaeoenvironmental conditions during the Baltic Yoldia stage in the Tallinn area, northern Estonia. *Quaternary International* **27**: 83–94.
- Lie Ø, Dahl SO, Nesje A *et al.* 2004. Holocene fluctuations of a polythermal glacier in high-alpine eastern Jotunheimen, central-southern Norway. *Quaternary Science Reviews* **23**: 1925–1945.
- Loizeau JL, Span D, Coppee V *et al.* 2001. Evolution of the trophic state of Lake Annecy (eastern France) since the last glaciation as indicated by iron, manganese and phosphorus speciation. *Journal of Paleolimnology* **25**: 205–214.
- Majewska R, Convey P, De, Stefano M. 2016. Summer Epiphytic Diatoms from Terra Nova Bay and Cape Evans (Ross Sea, Antarctica) – A Synthesis and Final Conclusions. *PLoS ONE* **11**: e0153254.
- McGhee R. 1976. Paleoeskimo Occupations of Central and High Arctic Canada. *Memoirs of the Society for American Archaeology* **31**: 15–39.
- Narancic B, Pienitz R, Chaplign B *et al.* 2016. Postglacial environmental succession of Nettilling Lake (Baffin Island, Canadian Arctic) inferred from biogeochemical and microfossil proxies. *Quaternary Science Reviews* **147**: 391–405.
- Oksanen J, Blanchet FG, Friendly M *et al.* 2019. vegan: Community Ecology Package. R package version 2.5-5. <https://cran.r-project.org/web/packages/vegan/index.html>
- Patzke M, Greenman JW, Ielpi A *et al.* 2018. Sedimentology of the sandstone-dominated units in the Fury and Hecla Basin, northern Baffin Island, Nunavut In *Summary of Activities 2018. Canada-Nunavut Geoscience Office*; 75–84.
- Pienitz R, Lortie G, Allard M. 1991. Isolation of lacustrine basins and marine regression in the Kuujuaq Area, Northern Québec, as inferred from diatom analysis. *Géographie physique et Quaternaire* **45**: 155–174.
- Pienitz R, Smol JP, Birks HJB. 1995. Assessment of freshwater diatoms as quantitative indicators of past climatic change in the Yukon and Northwest Territories, Canada. *Journal of Paleolimnology* **13**: 21–49.
- Rolland N, Larocque I, Francus P *et al.* 2008. Holocene climate inferred from biological (Diptera: Chironomidae) analyses in a Southampton Island (Nunavut, Canada) lake. *The Holocene* **18**: 229–241.
- Schilder J, van Hardenbroek M, Bodelier P *et al.* 2017. Trophic state changes can affect the importance of methane-derived carbon in aquatic food webs. *Proceedings of the Royal Society B: Biological Sciences* **284**: 20170278.
- Sim VV. 1960. A Preliminary account of late “Wisconsin” glaciation in Melville Peninsula, N.W.T.* *The Canadian Geographer/Le Géographe canadien* **4**: 21–34.
- Singh J, Singh RP, Khare R. 2018. Influence of climate change on Antarctic flora. *Polar Science* **18**: 94–101.
- Smith B, Wilson JB. 1996. A Consumer’s Guide to Evenness Indices. *Oikos* **76**: 70–82.
- Sobek S, Durisch-Kaiser E, Zurbrügg R *et al.* 2009. Organic carbon burial efficiency in lake sediments controlled by oxygen exposure time and sediment source. *Limnology and Oceanography* **54**: 2243–2254.
- Szabó B, Padisák J, Selmečzy GB *et al.* 2017. Spatial and temporal patterns of benthic diatom flora in Lake Stechlin, Germany. *Turkish Journal of Botany* **41**: 211–222.
- Walker DA, Reynolds MK, Daniëls FJA *et al.* 2005. The Circumpolar Arctic vegetation map. *Journal of Vegetation Science* **16**: 267–282.
- Wetzel RG. 2001. *Limnology: lake and river ecosystems*. Academic Press: San Diego.
- Zimmermann C, Poulin M, Pienitz R. 2010. *The Pliocene-Pleistocene freshwater flora of Bylot Island, Nunavut, Canadian High Arctic. Iconographia Diatomologica* **21**: 1–407.